Bessel-beam-written nanoslit arrays and characterization of their optical response

R. Sahin, Y. Morova, E. Simsek, and S. Akturk

Citation: Appl. Phys. Lett. **102**, 193106 (2013); doi: 10.1063/1.4805358
View online: http://dx.doi.org/10.1063/1.4805358
View Table of Contents: http://apl.aip.org/resource/1/APPLAB/v102/i19
Published by the American Institute of Physics.

Bessel-beam-written nanoslit arrays and characterization of their optical response

R. Sahin,[1] Y. Morova,[1] E. Simsek,[2] and S. Akturk[1,a)]
[1]*Department of Physics, Istanbul Technical University, Maslak 34469, Istanbul, Turkey*
[2]*Electrical and Computer Engineering, The George Washington University, 20052 Washington DC, USA*

(Received 22 January 2013; accepted 30 April 2013; published online 16 May 2013)

Nanoslit arrays are fabricated on thin metal film coated glass slides using femtosecond laser pulses with Bessel beam profiles. The optical properties of the fabricated structures with different periodicities are characterized with transmission spectroscopy. Experimental results reveal the existence of two separate surface plasmon resonance modes occurring at the metal-air and metal-glass interfaces. These two resonance modes cause two minima in the high transmission spectra of the sub-skin depth thick thin films in the visible and near infrared regions. The existence of double surface plasmon resonance modes is verified with additional experiments, theoretical and numerical studies. Due to its relaxed alignment constraints, reduced aberrations, scalability property to shorter wavelengths, and resulting shorter dimensions, nanofabrication with diffraction-free Bessel beams is an easy, cheap, and advantageous alternative to regular lithography techniques to fabricate nanoslit arrays. The shift of the resonance wavelength with a change in the refractive index of the surrounding medium can be exploited for enhanced sensing. © *2013 AIP Publishing LLC*. [http://dx.doi.org/10.1063/1.4805358]

Plasmonic structures are most commonly fabricated with lithographical methods. The direct writing through laser ablation can provide a faster and easier alternative.[1–3] Particularly, femtosecond (fs) pulsed lasers can yield fabrication resolution well below the laser wavelength by working near the ablation threshold.[4] In fs laser nanofabrication, beams must be focused tightly with corrected objectives to obtain smallest focal spots. Such high NA focusing requires meticulous alignment and can be prone to aberrations. It was recently demonstrated that using the diffraction-free Bessel beams can eliminate such practical difficulties.[5] Ablation resolution of about 200 nm is reached for both two-dimensional[5] and three-dimensional structures,[6] which is already sufficient for certain plasmonic applications.

The particular interest of this work is the transmission through sub-wavelength apertures, which has been one of the most interesting applications of plasmonics.[7,8] Excitation of surface plasmon polaritons (SPPs) by the incident electromagnetic radiation and re-coupling of polaritons to far field light waves yields extraordinary transmission when the resonance conditions are met.[9–11,13] In order to observe these enhancements, the apertures are usually generated on (nearly) opaque metal sheets, so that film transmission is negligible. In sensing and related applications, the shifts in the spectral transmission peaks provide the relevant information (i.e., change of refractive index).

In this work, we first demonstrate that the nanoslit arrays can be fabricated with fs laser Bessel beams and then investigate their optical properties as a function of wavelength, periodicity, and background. In our experiments, we work with partially transparent thin films, so that resonant excitation of surface plasmons cause drops in the transmission. Therefore, the sensitivity of spectral minima (instead of maxima in the case of opaque films) to the surface conditions can be exploited. Experimental results suggest that dual surface plasmon resonance (SPR) modes can be observed in such structures that might be instrumental for sensing applications. This scheme has particular advantages for situations in which high signal-to-noise ratio is needed.

This paper first explains the fabrication and characterization methods. Next, the experimental results obtained with transmission spectroscopy are provided. Finally, the experimental results are discussed under the light of theoretical and numerical results.

The thin gold films are deposited on glass substrate under a 10^{-7} mbar pressure with the help of a thermal evaporator. Chemically cleaned glass substrate is rotated during evaporation in order to increase homogeneity of the gold film. Evaporation rate is kept constant at 0.5 Å/s. Gold is evaporated to a thickness of 25 nm, with chrome (5 nm) used for adhesion. The chrome layer causes a small drop in total transmission and minimal change in the observed spectral features (see Fig. 3 below).

The laser source used for ablation is a chirped-pulse amplification system, producing 550-fs pulses at 1 kHz repetition rate, at a center wavelength of 1030 nm (Amplitude Systemes, s-Pulse). The third harmonic of the laser (343 nm wavelength) is generated through consequent second harmonic and sum-frequency generations. The laser energy is controlled with a waveplate and a polarizer. Gaussian laser output beam is converted to a Bessel beam with a 40°-base angle axicon. The sample is scanned under laser illumination by a piezo stage (Mad City Labs, Nano3D 200). Scan speed of the sample is kept constant at 50 μm/s. At these conditions, by decreasing the incoming laser energy, we are able to ablate stripes as narrow as 125 nm (with irregularities due to pulse to pulse instabilities). These stripes become uniform for width above 200 nm. By changing the distance orthogonal to

a)selcuk.akturk@itu.edu.tr

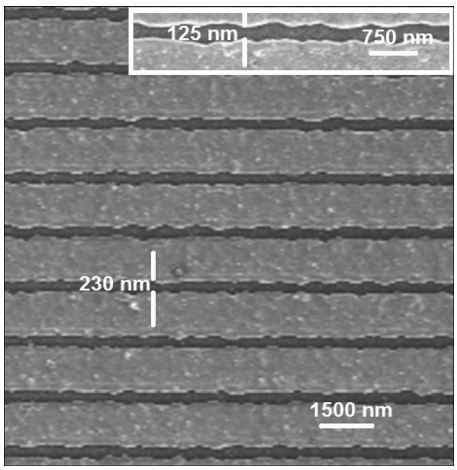

FIG. 1. SEM of a nanoslit array written by femtosecond laser Bessel beam ablation method. Darker regions are ablated stripes. The inset shows a stripe written close to the resolution limit.

ablation direction, nanoslit arrays are fabricated with different periods. The total extent of the nanoslit arrays is $50\,\mu\text{m} \times 50\,\mu\text{m}$. Fig. 1 shows a scanning electron micrograph (SEM) of one of the nanoslit arrays fabricated with the explained method.

For the characterization of the fabricated structures, transmission spectroscopy is performed in the spectral range of 400 nm–1100 nm, using a setup similar to one described in Fig. 2 of Ref. 14. The light source is a tungsten halogen lamp (StellarNet SL1), which is focused into an optical fiber. Fiber output is collimated by a microscope objective, goes through a Glan-Taylor polarizer, and illuminates the samples (from the metal side) at a diameter of 3 mm. The total power after the fiber is 0.4 mW. The illuminated samples are then imaged by a 20× objective. At the image plane, an iris is used to pass only the image of the array of interest. Finally, another objective is used behind the iris, to focus the transmitted light onto the fiber of the spectrometer (Avantes AvaSpec 3648). Since the detector of the spectrometer has a low response in the NIR, in order to reliably measure wavelengths beyond 1000 nm, we used a long-pass filter after the polarizer. The transmission spectra presented below are found by dividing the spectra measured through the nanoslit array by spectra measured without the sample.

In order to clarify the attribution of the observed spectral features to plasmonic effects, we measured transverse electric (TE) and transverse magnetic (TM) transmission spectra on four nanoslit arrays with periodicities of 550, 640, 860, and 980 nm. The results are plotted in Fig. 2.

As expected, there is no resonance behavior for the TE polarization. However, for the TM polarization we first observe a set of dips occurring at the wavelengths of 557, 639, 895, and 992 nm for p = 550, 640, 860, and 980 nm cases, respectively. According to the phase-matching condition for the TM mode obtained using plasmon dispersion relation[12]

$$\lambda_{SPR} = p\sqrt{\frac{\epsilon_d \epsilon_s}{\epsilon_d + \epsilon_s}}, \tag{1}$$

where λ_{SPR} and p are the SPR wavelength and grating period; ϵ_d and ϵ_s are the electrical permittivity values of dielectric

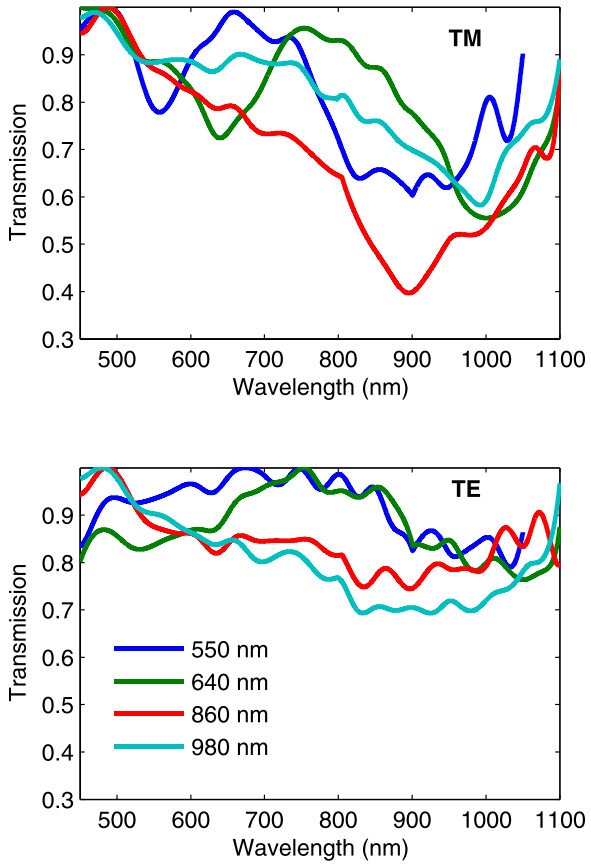

FIG. 2. Normalized transmission spectra through slit arrays for TM (top) and TE (bottom) polarizations.

background and metal, respectively; these dips are natural outcome of the SPPs excited on the gold-air interface. However, in Fig. 2 there are two additional dips occurring at the wavelengths of 900 and 1000 nm, for $p = 550$ and 640 nm cases, respectively. Motivated by existence of multiple SPR modes of the nanoparticle arrays fabricated on top of glass slides in Ref. 14, in Fig. 3, we plot SPR wavelength as a function of periodicity using Eq. (1) and assuming two different dielectric backgrounds (air and glass) and two

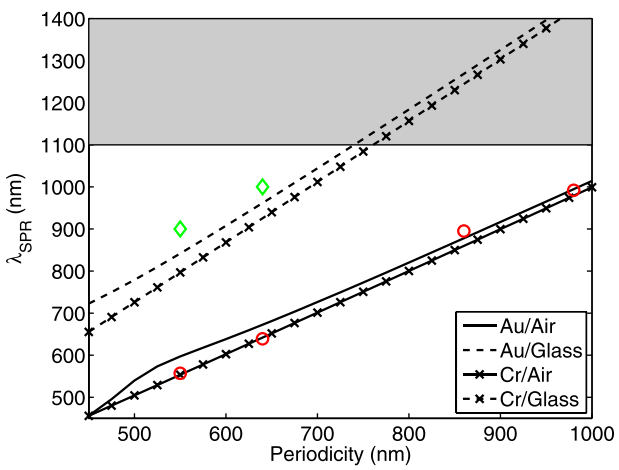

FIG. 3. Slit array period vs. SPR wavelength, calculated according to Eq. (1). Solid and dashed lines assume gold stripes situated in air and glass, respectively, whereas crossed solid and crossed dashed lines assume chromium stripes situated in air and glass, respectively. Red circles and green diamonds mark where the dips are in experimental results.

different metals (gold and chromium). For the optical constants of gold and chromium, the experimental values are used[17] rather than Drude model to eliminate any concern regarding the selection of appropriate values for plasmon and relaxation frequencies. The dielectric constant of the glass is taken as $\epsilon_{glass} = 2.13$ and $\epsilon_{air} = 1$ is used for air. When we mark the experimental results in Fig. 3, we realize that these secondary dips are the natural outcome of SPPs generated on the metal-glass interface.

Since the structure consists of 5 nm thick Cr and 25 nm thick Au stripes and these metals have SPR wavelengths very close to each other (see Fig. 3), it is not possible to conclude that the secondary SPPs are generated on Cr-glass or Au-glass interface, but we can safely say that SPPs are excited both on top and bottom surfaces of these stripes. In our numerical studies, as explained below, we observe that having a 5 nm of Cr underneath a 25 nm Au stripe array causes a broader transmission dip with respect to a 30 nm Au stripe array and again this can be explained by these metals having SPR wavelengths very close to each other.

In order to confirm the existence of dual SPP modes, we conduct another set of experiments by dropping glycerin on the metal film (including slit arrays) and placing a microscope coverslip on top of the drop. Hence, the slit arrays are sandwiched between glass and glycerin/coverslip, and both sides of the metal have roughly the same dielectric constant. Figure 4 shows transmission spectra for slit arrays of 500 nm and 810 nm periodicities. Before glycerin treatment, the metal-glass resonance of 500 nm case coincides with the metal-air resonance of 810 nm one. With the glycerine cover, the SPP modes excited on the metal-air interface of 810 nm case disappear, whereas the SPP mode excited on the metal-glass interface of 500 nm case remains almost the same (SPP mode on metal-glass interface of 810 nm case is always out of our spectral range). These results cross-validate each other and verify that metal stripe arrays excite SPPs on both top and bottom interfaces, as is also reported in Ref. 15.

Note that surface plasmons play different roles in the transmission through perforated thick metallic structures and transmission through ablated thin metallic films. For the former, enhanced transmission is observed at the resonance wavelength due to excitation of SPPs on the incidence interface, coupling of the charge oscillations to polaritons on the opposite interface, and finally coupling of the later plasmons to free space light.[9] These processes have a low efficiency, but since there is no light transmission otherwise, the enhancement becomes observable. For the latter, the film thickness is on the order of plasmon evanescent decay length in the perpendicular direction. Therefore, the incident light can directly excite SPPs on both interfaces. When the plasmons are excited, their energy comes from the incident light; as a result, the transmission drops at the resonance wavelength.

We also perform finite difference time domain (FDTD) calculations of the light transmission through nanoslit arrays fabricated on top of a glass slide and calculate the transmission spectra using Wavenology EM, a commercially available time domain solver. The dielectric constant of the glass and air is taken as above. As shown in the inset of Fig. 6, the metallic parts are modeled as gold and chromium rectangles with heights of 25 nm and 5 nm, respectively. The width of these rectangles is calculated with $w = p$–230 nm, where p is width of the periodic unit cell and 230 nm is the width of ablated region. Periodic boundary conditions are used at the $\pm y$ boundaries to account for the periodic nature of the nanoslit array. A grid spacing of 0.5 nm is employed. Again, the experimental values are used for the optical constants of gold and chromium.[17] The incident illumination is a p-polarized plane wave introduced from the glass side. Perfectly matched layers are applied at the $\pm z$ boundaries. Figs. 5(a) and 5(b) show the magnitude of the magnetic field passing through the arrays at the wavelengths of 740 nm and 800 nm for the $p = 500$ nm case. Agreeing well with the experiment results, the transmission at $\lambda = 740$ nm is much weaker than the transmission at $\lambda = 800$ nm.

Finally, we calculate the shift of the resonance wavelength (transmission minima) as a function of the dielectric constant of the background medium to investigate the potential of the fabricated structures for sensing. We follow the procedure used to generate Fig. 5 assuming $\epsilon_1 = \epsilon_2 = \epsilon_r$. As shown in Fig. 6, in the p = 500 nm case, the SPR wavelength of structure changes from 732 nm to

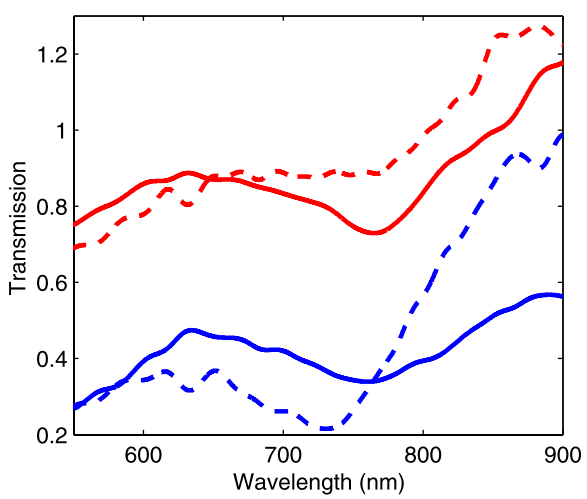

FIG. 4. Transmission spectra through slit arrays in air and glycerin, for TM polarized light. Blue and red curves correspond to 500 nm and 810 nm periods, respectively. The dashed curves are obtained after glycerine treatment, and these two spectra are shifted for clarity.

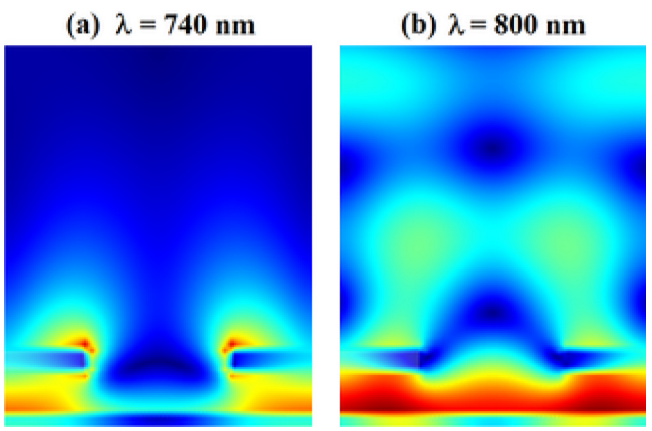

FIG. 5. Magnitude of the magnetic field at $-120 < z < 480$ nm, $-240 < y < 240$ nm, where gold-chromium stripes are located at $0 < z < 30$ nm, for the p = 500 nm case (a) $\lambda = 740$ nm and (b) $\lambda = 800$ nm.

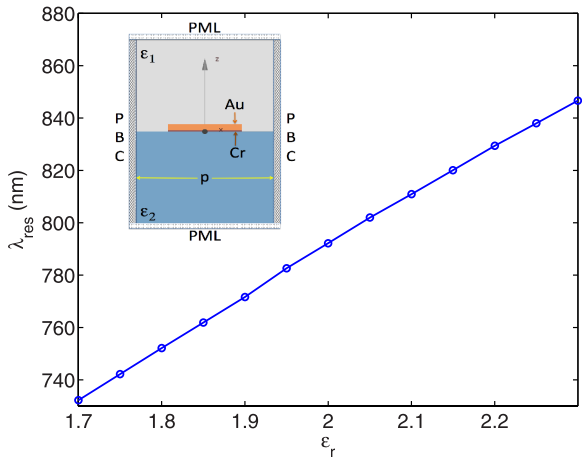

FIG. 6. Shift of SPR resonance wavelength with periodicity for the p = 500 nm case with 25 nm thick, 270 nm wide gold stripes.

847 nm as the dielectric constant of the background medium changes from 1.7 to 2.3. This means a sensitivity of 540 nm/RIU (refractive-index unit), which is comparable with experimental results of plasmonics sensors found in the literature.[15,16] Note that here we experience a very high transmission at a wide range of wavelengths, differing from structures with perforated thick metal layers. For sensing applications, the relative change in intensity close to the SPR is used for detection. Therefore, our scheme might be extremely useful for the plasmonic sensor applications where the signal-to-noise ratio is low.

In conclusion, femtosecond pulses with Bessel beam profiles are used to generate nanoslit arrays on semi-transparent metal thin films, and optical characterization with transmission spectroscopy clearly indicates that SPPs are excited on both top and bottom surface of the metal stripes. The shift of minima observed in the measured spectra with respect to the dielectric constant of the layer above the metal can be exploited for sensor applications. As compared to similar approaches in the literature, our scheme yields orders of magnitude larger total transmissions; therefore, it would be suitable and advantageous for low signal-to-noise ratios and better sensitivity requirements.

This work was supported by Scientific and Technological Research Council of Turkey (TUBITAK, Grant No. 110T330) and Turkish Academy of Sciences (TUBA GEBIP). R. Sahin also thanks TUBITAK for Ph.D. scholarship.

[1]Y. Nakata, T. Okada, and M. Maeda, Appl. Phys. A **79**, 1481–1483 (2004).
[2]S. Eliezer, N. Eliaz, E. Grossman, D. Fisher, I. Gouzman, Z. Henis, S. Pecker, Y. Horovitz, M. Fraenkel, S. Maman, and Y. Lereah, Phys. Rev. B **69**, 144119 (2004).
[3]A. V. Kabashin, M. Meunier, C. Kingston, and J. H. T. Luong, J. Phys. Chem. B **107**, 4527–4531 (2003).
[4]A. P. Joglekar, H. Liu, E. Meyhfer, G. Mourou, and A. J. Hunt, Proc. Natl. Acad. Sci. U.S.A. **101**, 5856–5861 (2004).
[5]B. Yalizay, T. Ersoy, B. Soylu, and S. Akturk, Appl. Phys. Lett. **100**, 031104–0311043 (2012).
[6]F. Courvoisier, J. Zhang, M. K. Bhuyan, M. Jacquot, and J. M. Dudley, "Applications of femtosecond Bessel beams to laser ablation," Appl. Phys. A (to be published).
[7]T. W. Ebbesen, H. J. Lezec, H. F. Ghaemi, T. Thio, and P. A. Wolff, Nature (London) **391**, 667–669 (1998).
[8]C. Genet and T. W. Ebbesen, Nature (London) **445**, 39–46 (2007).
[9]W. L. Barnes, A. Dereux, and T. W. Ebbesen, Nature (London) **424**, 824–830 (2003).
[10]J. A. Porto, F. J. Garca-Vidal, and J. B. Pendry, Phys. Rev. Lett. **83**, 2845–2848 (1999).
[11]H. F. Schouten, N. Kuzmin, G. Dubois, T. D. Visser, G. Gbur, P. F. A. Alkemade, H. Blok, G. W. t Hooft, D. Lenstra, and E. R. Eliel, Phys. Rev. Lett. **94**, 053901 (2005).
[12]S. A. Maier, *Plasmonics: Fundamentals and Applications* (Springer, 2007).
[13]E. Devaux, T. W. Ebbesen, J.-C. Weeber, and A. Dereux, Appl. Phys. Lett. **83**, 4936 (2003).
[14]K. B. Crozier, E. Togan, E. Simsek, and T. Yang, Opt. Express **15**, 17482–17493 (2007).
[15]K.-L. Lee, C.-W. Lee, W.-S. Wang, and P.-K. Wei, J. Biomed. Opt. **12**, 044023 (2007).
[16]A. G. Brolo, R. Gordon, B. Leathem, and K. L. Kavanagh, Langmuir **20**, 4813–4815 (2004).
[17]A. D. Rakic, A. B. Djurisic, J. M. Elazar, and M. L. Majewski, Appl. Opt. **37**, 5271–5283 (1998).